Theoretical and Experimental Stress Analysis of Cam With Simple Harmonic Motion

Aveen Ahmed Abdulkareem
Teaching Assistant
College of Engineering – University of Baghdad
email: av_mechanics@yahoo.com

ABSTRACT

Cams are considered as one of the most important mechanical components that depends the contact action to do its job and suffer a lot of with drawbacks to be predicted and overcame in the design process. this work aims to investigate the induced cam contact and the maximum shear stress energy or (von misses) stresses during the course of action analytically using Hertz contact stress equation and the principal stress formulations to find the maximum stress value and its position beneath the contacting surfaces. The experimental investigation adopted two dimensions photoelastic technique to analyze cam stresses under a plane polarized light. The problem has been numerically simulated using Ansys software version 15 as FE solver and depending on Lagrange and Penalty contact algorithm. The effect of cam geometry, characterized by some parameters such as follower radius, face width, rise and return angles, and modulus of elasticity on the contact stress is investigated aiming to minimize the induced stresses.

Key words: Cam modeling, contact stress, photoelastic experimental stress analysis

تحليل الإجهادات نظرياً وعملياً للحدبات ذات الحركة التناغمية البسيطة

أفين أحمد عبد الكريم
مدرس مساعد
كلية الهندسة ـ جامعة بغداد

الخلاصة

تعتبر الحدبات كواحدة من اهم العناصر الميكانيكية التي تعتمد فعل التلامس للقيام بوظيفتها وتعاني العديد من المعوقات التي يجب تنبأها والتغلب عليها في عمليات التصميم. يهدف هذا العمل لتحري اجهادات التلامس واجهادات طاقة القص العظمى خلال العمل نظريا باستعمال معادلة اجهادات التماس لهيرتز وعلاقات الاجهادات الاساسية لايجاد قيمة الاجهاد الاعظم وموقعة تحت سطوح التلامس . التحري العملي اعتمد تقنية المرونة الضوئية ثنائية البعد لفحص اجهادات الحدبة تحت الضوء مستوي الاستقطاب. تمت محاكات المشكلة عدديا باستخدام برنامج Ansys النسخة الخامسة عشر كمحلل عناصر محدد بأعتماد خوارزمية (Lagrange and penalty) . تم تحري تأثير شكل الحدبة , مميزا بمجموعة من العوامل كنصف قطر الحدبة وعرض الوجه وزوايا الصعود والنزول ومعامل المرونة , على إجهاد التماس بهدف تقليل الاجهادات المتولدة .

الكلمات الرئيسية : نمذجة الحدبة , اجهاد التماس ,تحليل الاجهاد ضوئيا **.**

1 .INTRODUCTION

Power and movement transmission are regarded as the principle of the mechanical engineering duties which contribute the modern life appearance. Gears, belts, sprockets and cams are the most common used mechanical elements for such purpose. In general the work of such elements is accompanied by some problems like power loss, heat generation, wear, fatigue, high induced contact and bending stresses. Cam may be defined as a machine element with a curved outline or a curved groove, which, by its oscillation or rotation motion, gives a predesigned motion to another element called the follower and has very important function especially in the printing presses, shoe machinery, textile machinery, gear-cutting machines, and screw machines. In any class of machinery in which automatic control and accurate timing are paramount, the cam is an indispensable part of mechanism **Anvoner, 1959.** This work will spot the light on the cam stresses affected by some geometrical parameters such as rise and return angles, face width. The role of modulus of elasticity will be taken into account in this study. Hertz contact stress equation for nonconforming bodies will be adopted as the analytical solution and examined how far the problem will obey Hertz equation. The interaction of the cam and its follower will be numerically simulated using Ansys software version 15 as a FE solver to investigate the different stresses values and distributions. The plane polarized light and photoelastic stress analysis technique will be used in order to compare the accuracy and the similarity between the assumed conditions, for the analytical and numerical, and the applied one on the experimental test and how amount of discrepancy will be produced.

2. Cam Mathematical Representation

The simplicity of cam manufacturing methods and its traditional use associated by the good performance, leads the researchers and the manufacturers to evolve cam shape and work and there are a lot of cam types which could be classified according to the follower motion relative to the cam rotational axis as:

1. Cylindrical cams.
2. Radial cams.

Another classification depends on the follower motion and divides cams into:

1. Uniform velocity.
2. Simple harmonic motion.
3. Uniform acceleration and retardation.
4. Cycloidal motion.

The precise geometrical representation is considered as the first step of any simulation or investigation to grantee the accurate and dependable results. The studied cam in this work is the harmonic displacement one and its profile characterized by the rising distance, base radius, and the different course angles where **Oberg, et al., 2000.**

$$r(\theta) = r_b + \frac{S}{2}\left(1 - cos\frac{\pi\theta}{\beta}\right) \tag{1}$$

While the follower velocity and acceleration is

$$v(\theta) = \frac{S\pi\omega}{2\beta} \sin\frac{\pi\theta}{\beta} \tag{2}$$

$$a(\theta) = \frac{S}{2}(\frac{\pi\omega}{\beta})^2 \cos\frac{\pi\theta}{\beta} \tag{3}$$

Where r is the cam profile radii, r_b is the cam base radius, S is the max. follower rise distance, $\boldsymbol{\beta}$ is the rising, dwell or falling angle as shown in **Fig. 4**, v is the follower velocity, and a is the acceleration.

Eq. (1) has been programmed using quick basic 64 to calculate the different profile radii and their angles. Each cam profile was presented by 180 points to ensure a realistic representation able to simulate the real cam shape. These points are feed to the FE solver as a key points and connected by a spline to construct the area and then the two dimensional model will be extruded to generate the 3 dimensional model.

3. THEORITICAL STRESS ANALYSIS

3. 1 Analytical Stress Analysis

The contact of the mechanical elements has the functional key role in their interaction, regarding power and movement transmission, and depends on the relative sliding and rolling action. Its relatively large contacting area and zero relative sliding movement makes the conforming contact cases works with low contact stress levels comparing to its counterpart cases i.e. the nonconforming contact problems. In the 19th century Heinrich Hertz proposed his famous equation to calculate the contact pressure of the nonconforming contacting surfaces and dealt with as the governing equation till now days. The most important assumptions that must be taken into account to ensure genuine results are that the two bodies are continuous of constant curvature radius and the contacting area is small compared to the other dimensions. The contact stress has been found as a function of the applied normal load, the face width of the contacting bodies, the two bodies radius of curvature, and the material properties **Hearn 2001**.

$$P_{max} = \sqrt{0.35 \, \frac{F}{t} \times \frac{\left(\frac{1}{r_c}+\frac{1}{r_f}\right)}{\left(\frac{1}{E_c}+\frac{1}{E_f}\right)}} \qquad (4)$$

Where σ_c is the contact stress, F is the applied load, t is the face width, r_c and r_f are the cam and the follower radius of curvature at the contact zone, E_c and E_f are the modulus of elasticity for the cam and follower

And the mating bodies contacting area characterized by a rectangular area with its length equal to the face width t, while the other dimension could be calculated by the following formula

$$b = 1.076 \sqrt{\frac{F \times \left(\frac{1-v_c{}^2}{E_c}+\frac{1-v_f{}^2}{E_f}\right)}{t \times \left(\frac{1}{r_c}+\frac{1}{r_f}\right)}} \qquad (5)$$

The previous equations assumed the contacting elements to be cylinders.

The principal contact stresses at the contacting zone could be evaluated as following **Johnson 2003**.

$$\sigma_1 = \sigma_y = -P_{max}\left[\sqrt{\frac{y^2}{b^2}+1}\right]^{-1} \qquad (6)$$

$$\sigma_2 = \sigma_x = P_{max}\left[\left(2 - \left(\frac{y^2}{b^2}+1\right)^{-1}\right) \times \sqrt{\frac{y^2}{b^2}+1} - 2\left|\frac{y}{b}\right|\right] \qquad (7)$$

$$\sigma_3 = \sigma_z = -2vP_{max}\left[\sqrt{\frac{y^2}{b^2}+1} - \left|\frac{y}{b}\right|\right] \qquad (8)$$

While the shear stresses are

$$\tau_1 = \left|\frac{\sigma_2 - \sigma_3}{2}\right|, \tau_2 = \left|\frac{\sigma_1 - \sigma_3}{2}\right|, \tau_3 = \left|\frac{\sigma_1 - \sigma_2}{2}\right| \qquad (9)$$

Due to the applied load and material elastic behavior the contacting surfaces deformed elastically leading to minimize the center distance of the two bodies.

3. 2 Finite Element Approach

Unfortunately the most applicable differential equations governing the engineering and physical applications are complex, and have long term solutions so that the finite element approach has been adopted as a simple alternative way solving the most complex problems directly with a worthless error margin overcoming all the past time investigation techniques. The basic principle of the FEM is to discrete the general problem into a certain number of simple problems diminishing the time consume, efforts and cost. Dealing with FEM needs some experience and a well knowledge to the analytical background of the problem under concern because the results will come under any circumstances and it may be scattered or incorrect. The reliable and accurate results of the FEM depends on a lot of parameters such as the right simulation to the real working conditions like the applied load, the constraint, the working temperature and the right material properties such as the modulus of elasticity and poisson's ratio, as well as the accurate geometrical representation. The 3-D cam model has been built up in the FE environment, the material properties are setup as a structural of linear isotropic material with modulus of elasticity equal to 200 GN/m^2, 0.3 poisson's ratio, and density of 7830 Kg/m^3. The suitable element type and number have been chosen according to the convergence test. In general the larger element numbers the more accurate results but that leads to a long solution time so that the element number must be as small as possible to satisfy the solution. The applied load and constraint must be the same during the convergence test and by choosing a solid brick element 186 as the mesh element and by changing the element number and solve the problem again and again with different element numbers until there will be stabilized then this is the right element number. The best element type has been found to be solid brick element of 20 nodes and the adequate element number is 7555 including 450 contact surface elements and 375 contact target elements and the contact is frictionless **Akkamahdev 2015**. The target is chosen to be the follower while the contact surface is the cam and the applied load is 100 N distributed along the unity follower face width. The adopted contact algorithm approach is the Lagrange and penalty method.

4. Experimental Test

Almost engineering inventions and designs are part of the virtual world and haven't judged to engage the real working environment till it verified to be fully functional with comfortable safety especially for human related applications, high cost products, and mass production. Such critical decision couldn't be taken unless there is evidence support the claims of the vendor or designer, which is the experimental model.

    The previous analysis of the cam contact and principal stresses are withdrawn analytically depending on Hertz equations which has some assumptions must be followed to ensure the results accuracy.

    The experimental analysis will be conducted using the photoelastic technique to verify if the real cam induced stresses matches that of the analytical equations. The experimental cam model has been manufactured from the PSM-4 photoelastic sheet under a plane polarized light. The material properties such as modulus of elasticity and fringe value are investigated experimentally depending upon Euler's theory and bending test for a specimen cut from the same material **Helena Jin et.al. 2014** see **Fig.1**

$$EI \frac{\partial^2 y}{\partial x^2} = M \tag{10}$$

where

$$M = \left[\frac{wl}{2} + \frac{F}{2}\right] x - \frac{wx^2}{2} \tag{11}$$

Integrating the equation twice and applying the boundary condition's leads to

$$E = \frac{1}{I\delta} \left(-\frac{5}{384} wl^4 - \frac{1}{48} Fl^3\right) \tag{12}$$

Where w= 0.03 kg, l= 150 mm, h= 16 mm, t= 6 mm

    By increasing the applied load gradually and measuring the resulting deflection using dial gauge and adopting these values (load and deflection) in Eq.(12) a set of the modulus of elasticity will be calculated and then averaged to get a reliable modulus value **, Table 1** illustrates the test results

The fringe value will be investigated using the four point test or the pure bending test **James and William 1991**. where

$$\sigma_1 - \sigma_2 = \frac{N f}{t} \tag{13}$$

For pure bending

$$\sigma_1 = \sigma_x = \frac{MY}{I} = \frac{6M}{t \times h^2}$$

$$\therefore 937.5 \, \frac{F}{N} = f \tag{14}$$

Where N is the fringe order, f is the fringe value. **Fig. 2** and **Fig. 3** show the specimen dimensions and position of the applied load as well as the resulting fringe pattern. The applied load and the resulting fringe order are listed in **Table 2**.

The resulting average modulus of elasticity is (4.1 MN/m^2), and the average fringe value is 230 N/ (m. fringe order).

The experimental cam model has been shown in **Fig. 4** which has 50 mm base radius, 25 mm stroke distance, 15 mm for the follower radius, and 6 mm thickness. The cam shape has been modeled depending on Eq. (1) with rise, return, and upper dwell angle equal to 60°.

5 RESULTS AND DISCUSSION

The most important note to be mentioned at the first is that the applied load is 100 N, the base radius =50 mm, the follower radius is 15mm unless referred by other value, the face width is unity or clarified for different value, the modulus of elasticity is 200 GPa for cam and follower and showed for different values.

5.1 Analytical Results

According to the Hertz contact stress and area equations the results have been shown in **Fig. 5** and **Fig. 7**. It is clear that the contact stress decreased as a result of the increasing of the angular position and then return to its initial value while the contact area trends to behave in counter way and the cause behind such behavior is the variation of the radius of curvature as shown in **Fig. 6** which change from 50 mm at the base region to be 75 mm at the upper dwell region. It is evident that the follower of larger radii well enhances the contact stress values and that returned to the high contact area associated with the larger follower.

Fig. 8 implies the contact principal stresses distribution into the cam and how it decreases along the two contacting surfaces normal. The first and second max. principal stresses are equal to the max. contact stress at the contacting surfaces while the von mises equal to one sixth of the contact stress.

Fig. 9 shows the max. contact stress values for different cam face widths and for several follower radii. The increasing of the follower radius and cam face width increases the width and the length of the contact area respectively leading to decrease the max. induced stress.

Fig. 10 relates the effect of the cam and follower modulus of elasticity to the max. contact stress and clarify its increasing negative role for cam and follower, because the higher modulus means a lower deformation ability leading to lower contact area , where E_R is the ratio of the follower modulus of elasticity to that of the cam.

5.2 Numerical Results

The max principal stress in **Fig. 11** has max compressive value of 552 MPa and it is equal to the max. contact stress shown in **Fig. 12** , these results conform the results shown in **Fig. 5** and **Fig. 8**. The distribution of the von mises stress is shown in **Fig.13** with its max value equal to 408 MPa and equal to 0.7 of the max contact stress and that confirm the results in **Fig.8**. the distribution of the normal deformation within the cam and follower domain is shown in **Fig.14**

5.3 Experimental Results

The photoelastic pattern of stress analysis for three loaded cases are shown in **Fig.15**. The applied load are (a) 0.2, (b) 0.3, (c) 0.4 Kg and (d) is also 0.2 Kg but with scale 1:1, the resulting pattern are shown in the three figures. Depending upon Eq. (13) the left hand side could be gotten from Eq's. (6,7) by substituting the equivalent depth to the fringe order and find the difference between the 1st and 2nd principal stresses. **Table 3** summarized the experimental and theoretical results with the error percentage for the three cases.

The experimental principal stress differences have been measured depending on **Fig. 15** for the three loading cases by measuring the fringe orders and its y position. The Nth order will be substituted in Eq.(13) to find the experimental measurements as in fifth column in **Table 3** while the measured y values are substituted in Eq's. (6,7) to evaluate the theoretical first and second principal stresses (6th and 7th columns in **Table 3**) in terms of Eq's. (4,5) which in turn have been calculated for the same experimental loads of **Table 3**. The theoretical principal stress differences have been listed in 8th column. The experimental and theoretical results percentage error have been shown in the last column.

The max percentage of error is 10% and justified by the manufacturing and calibration errors.

6. CONCLUATION

From the whole results there are some concluding remarks which can be withdrawn such.

Follower radius plays the key role in controlling the contact stress because of its smaller value and its variation will not affect the stroke. The low levels of modulus of elasticity

minimize the chances of contact failure. The larger radius of curvature leads to smaller contact stress for both of the mating surfaces. Increasing the face width has a positive effect on the contact stress reduction. The max. principal stress at the contacting surfaces equal to the max. contact stress while von mises equal 0.6. The increasing of the applied load do not always leads to generate more photoelastic pattern but always shift them away of the contacting surfaces

REFRENCES

➢ Anvoner S. , 1959, *Theory of machines*, book.

➢ Akkamahdev G Chanagond., Raut L. B. 2015, *Finite Element Analysis of Roller Cam by Optimization of Surface Contact Area,* International Journal of Advanced Engineering Research and Studies.

➢ Hearn E. J, 2001, *Mechanics of Materials 2*,book, Third edition.

➢ Johnson, K, L, 2003, *Contact mechanics*, book

➢ James W. Dally, William F. Riley, 1991, *Experimental stress analysis*.

➢ Oberg Erik, Franklin D. Jones, Holbrook L. Horton, and Henry H. Ryffel, 2000, *Machinery's Handbook*, 26th Edition.

➢ Helena Jin, Cesar Sciammarella, Sanichiro Yoshida, Luciano Lamberti, 2014, *Advancement of Optical Methods in Experimental Mechanics*, Book, Volume 3.

NOMENCLATURE

b : contact zone half width (m).

E_c , E_f : cam and follower Modulus of elasticity , respectively (N/m^2).

F : applied load (N).

f : fringe value.

I : second moment of area (m^4).

L : length (m).

N : fringe order.

P_{max} : maximum contact pressure (N/m^2).

r_b : base radius of cam (m).

r_c , r_f : cam and Follower radius of curvature , respectively (m).

S : cam stroke (m).

t : face width (m).

v : follower velocity (N/m).

a : follower acceleration (m/s^2).

θ : angular position (degree).

σ_1 , σ_2, σ_3 : principal stress (N/m^2).

σ_c : contact stress (N/m^2).

v_f , v_c : poisson's rations.

τ_1 , τ_2 , τ_3 : principal shear stress(N/m^2).

δ: maximum beam deflection (m).

β : rising or falling angle (degree).

Table 1. Experimental modulus of elasticity

Mass(g)	100	200	300	400	500	600
δ (mm)	0.32	0.615	0.88	1.15	1.52	1.95
E (MN/m^2)	$3.8981*10^6$	$4.0566*10^6$	$4.2525*10^6$	$4.3388*10^6$	$4.1033*10^6$	$3.8401*10^6$

Table 2. Experimental fringe value

Load (F), N	Fringe Order (N)	Fringe Value (f)
0.245	1	229.68
0.49	1.9	241.77
0.74	3.1	222.27
0.981	4	229.68

Table 3. Experimental and theoretical cam stresses

P(Kg)	N	y'(scale depth) (mm)	y (real depth) (mm)	N*f/t (N/m^2)	$\sigma_{1\ theoretical}$ (N/m^2)	$\sigma_{2\ theoretical}$ (N/m^2)	$(\sigma_1 - \sigma_2)$ theoretical	Error %
0.2	1	14	4.375	38333.33	-43138.85	-1089.35	42049.5	8.8
	2	5	1.5625	76666.67	-93827.047	-14111.9	79715.179	3.97
0.3	1	25	7.8125	38333.33	-37195.462	-453.744	36741.718	4.3
	2	9	2.8125	76666.67	-89933.846	-7320.69	82613.157	7.1
	3	4.4	1.375	115000	-133969.77	-31610.7	102359.07	10
0.4	1	46	10.22	38333.33	-38112.201	-364.1857	38476.387	0.38
	2	21	4.6667	76666.67	-78091.454	-3342.614	81434.072	5.8
	3	13	2.889	115000	-112677.27	-11152.02	123829.28	7.1

Figure 1. Pure bending test specimen.
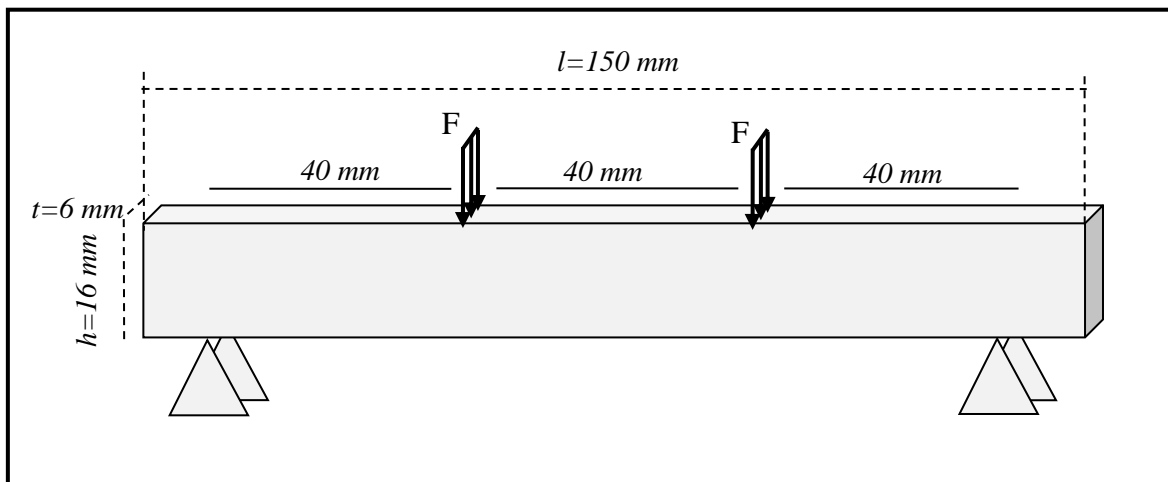
Figure 2. Dimension of pure test specimen with the position and value
of the applied load
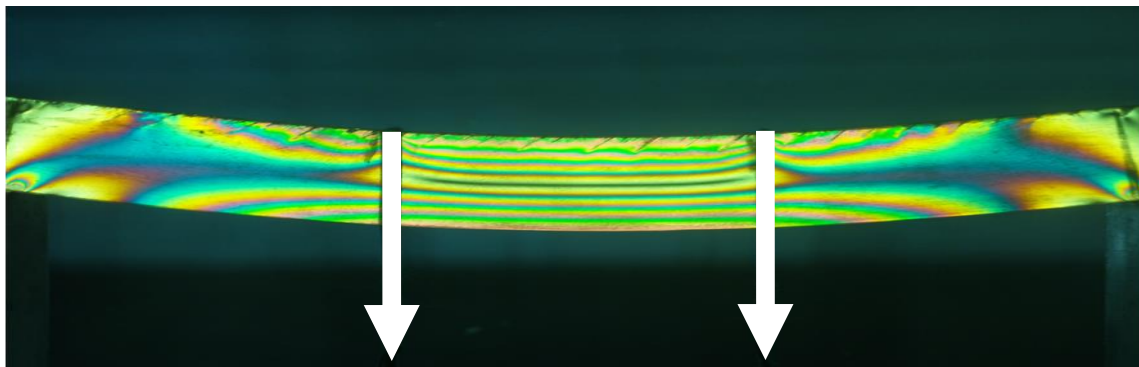
Figure 3. Photoelastic pure bending stress fring test
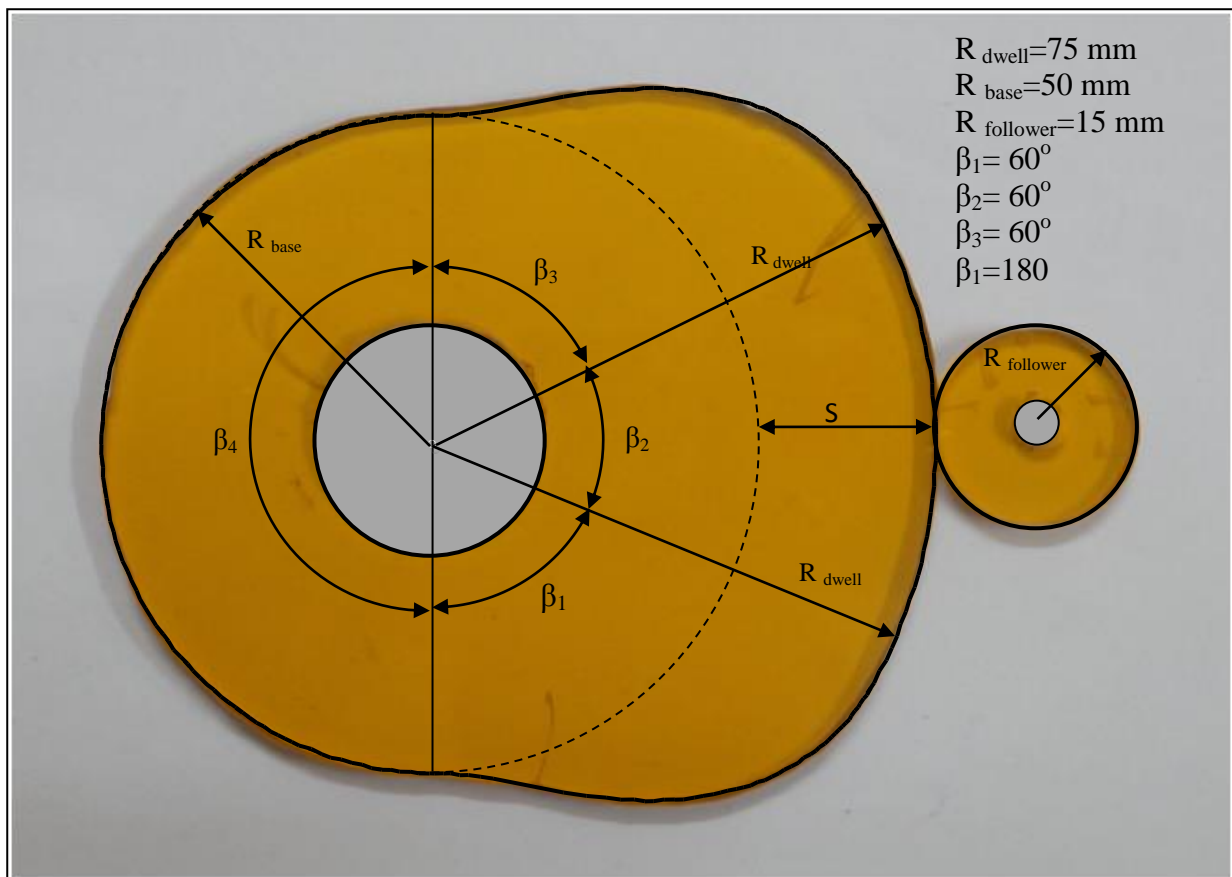
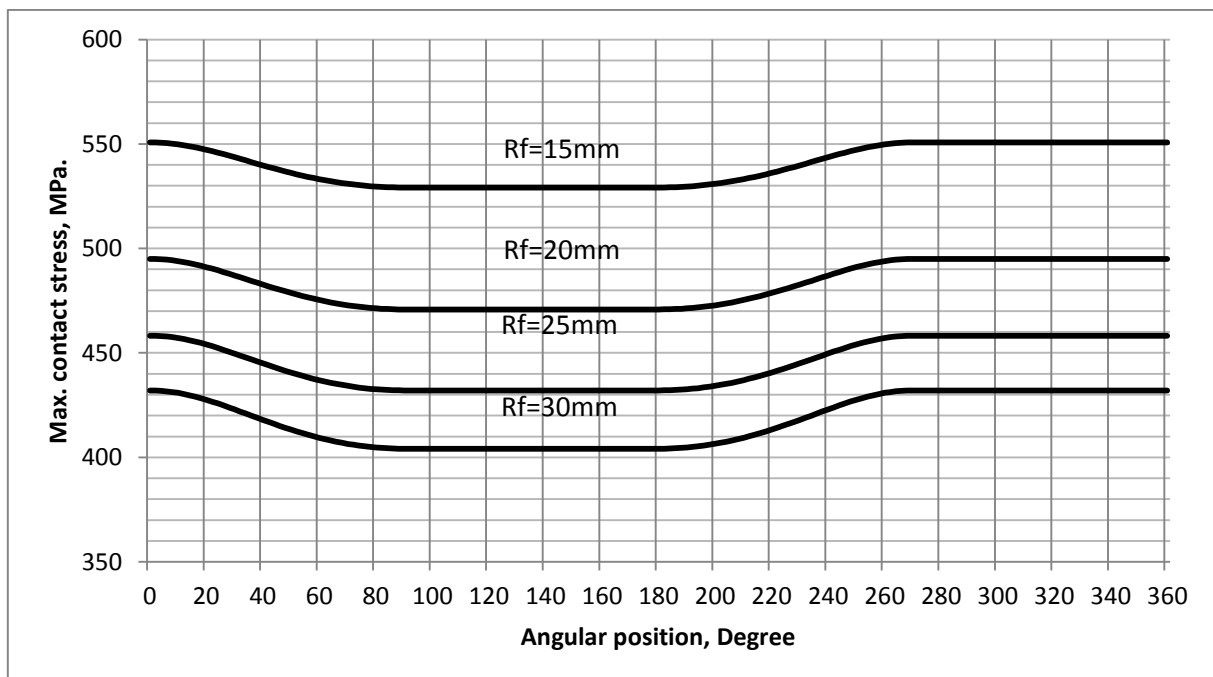**Figure 4.** Experimental photoelastic cam and follower model

Figure 5. The variation of the contact stress with angular position for different follower radii
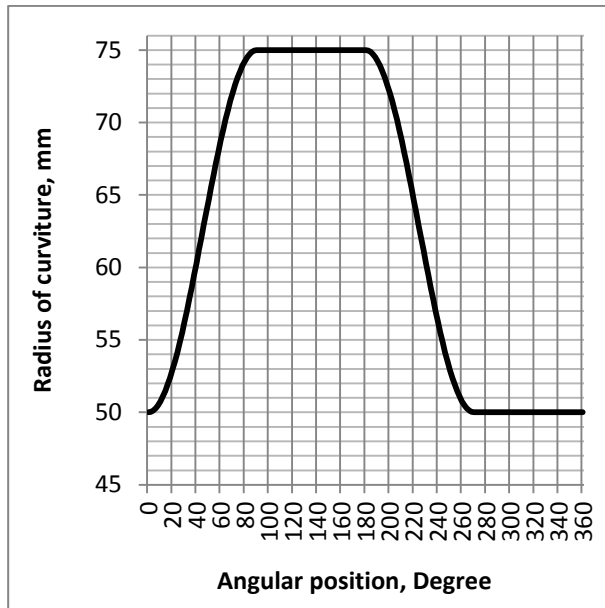
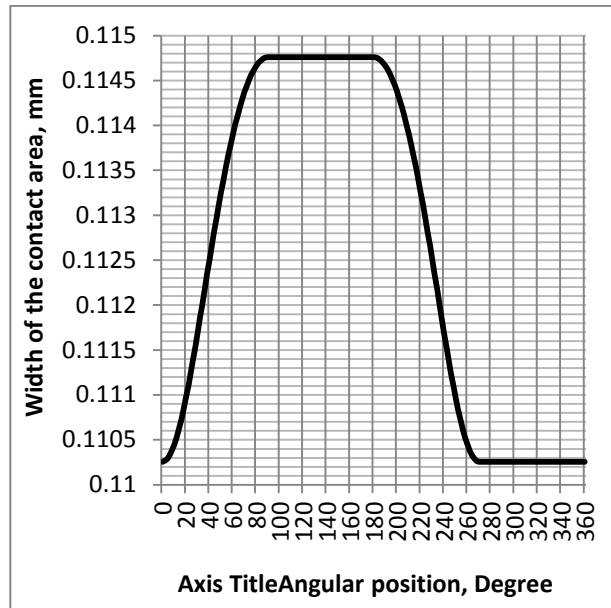**Figure 6**. The variation of the cam radius with respect to the angular position

Figure 7. The contact zone half width dimension change with the angular position
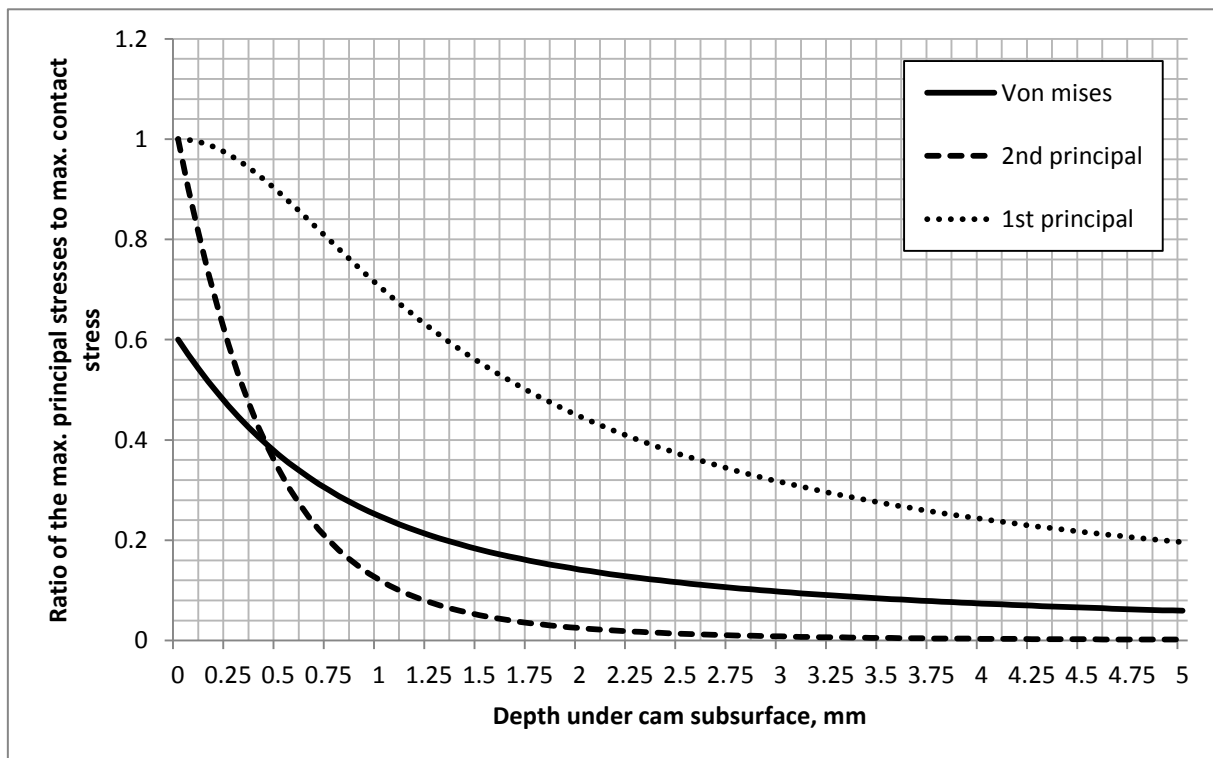
Figure 8. The ratio of the different principle stresses to the maximum contact pressure

211
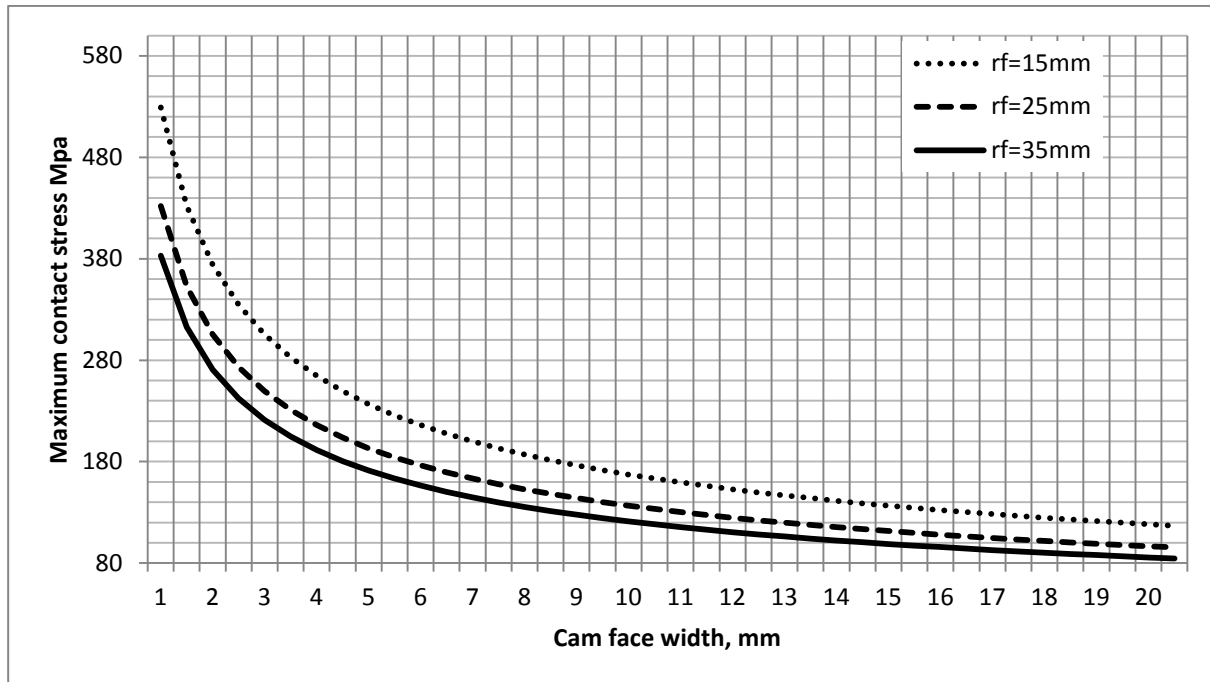
Figure 9. Trace the effect of the cam face width on the maximum contact stress
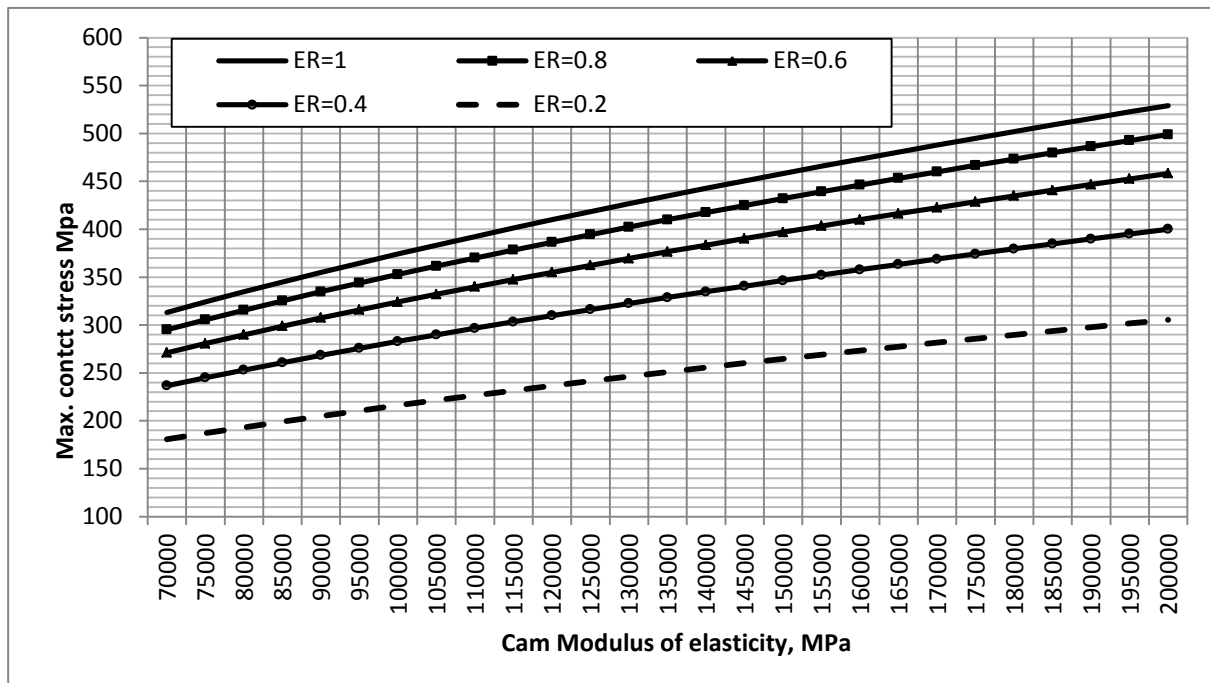
Figure 10. Variation of the maximum contact stress with the change of the modulus of elasticity
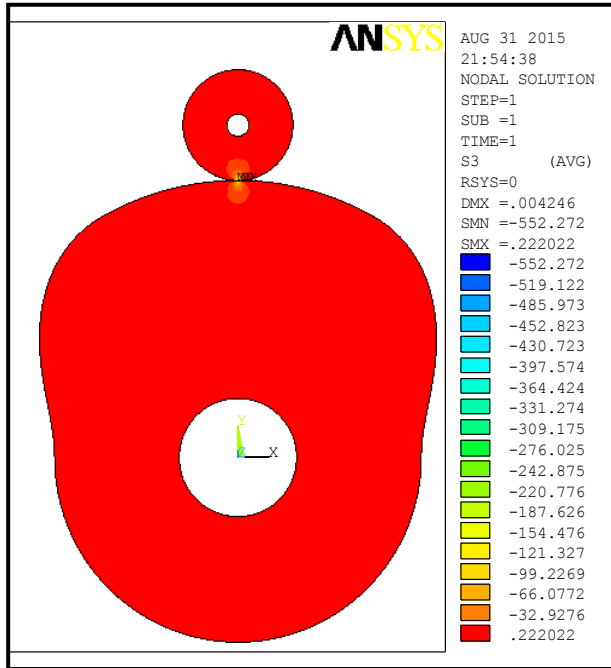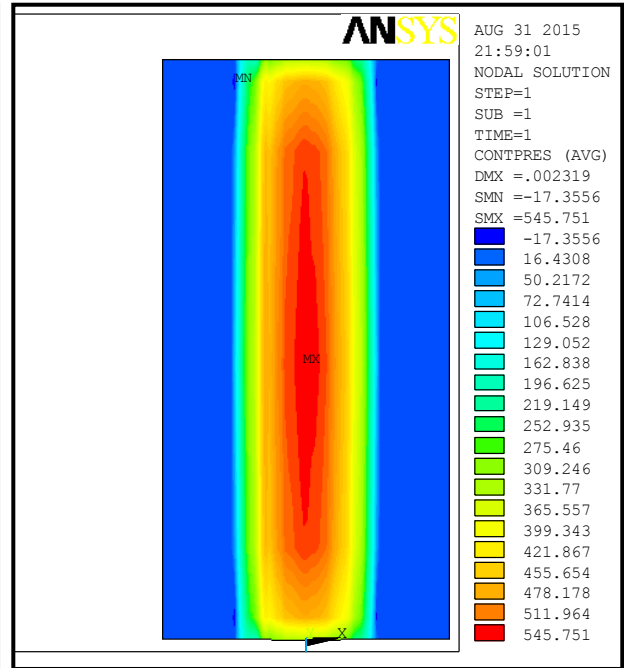
Figure 11. Maximum principal stress

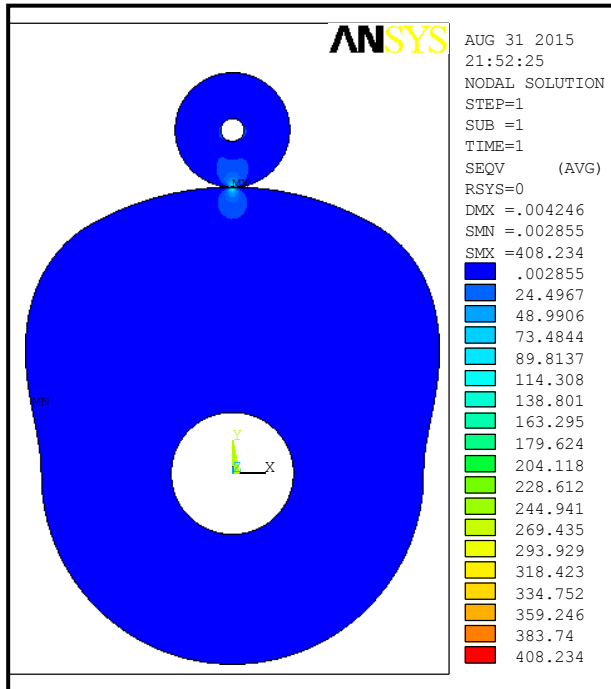**Figure 12.** Contact area and contact stress distribution

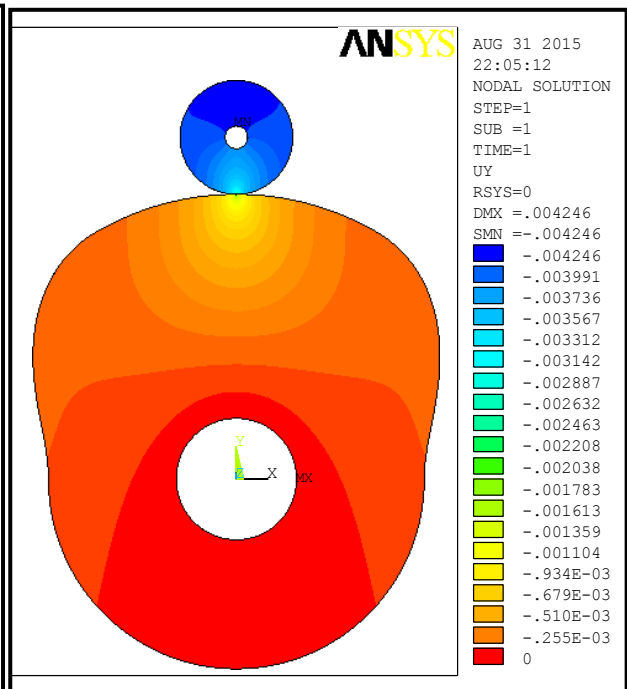**Figure 13.** Von mises stress distribution

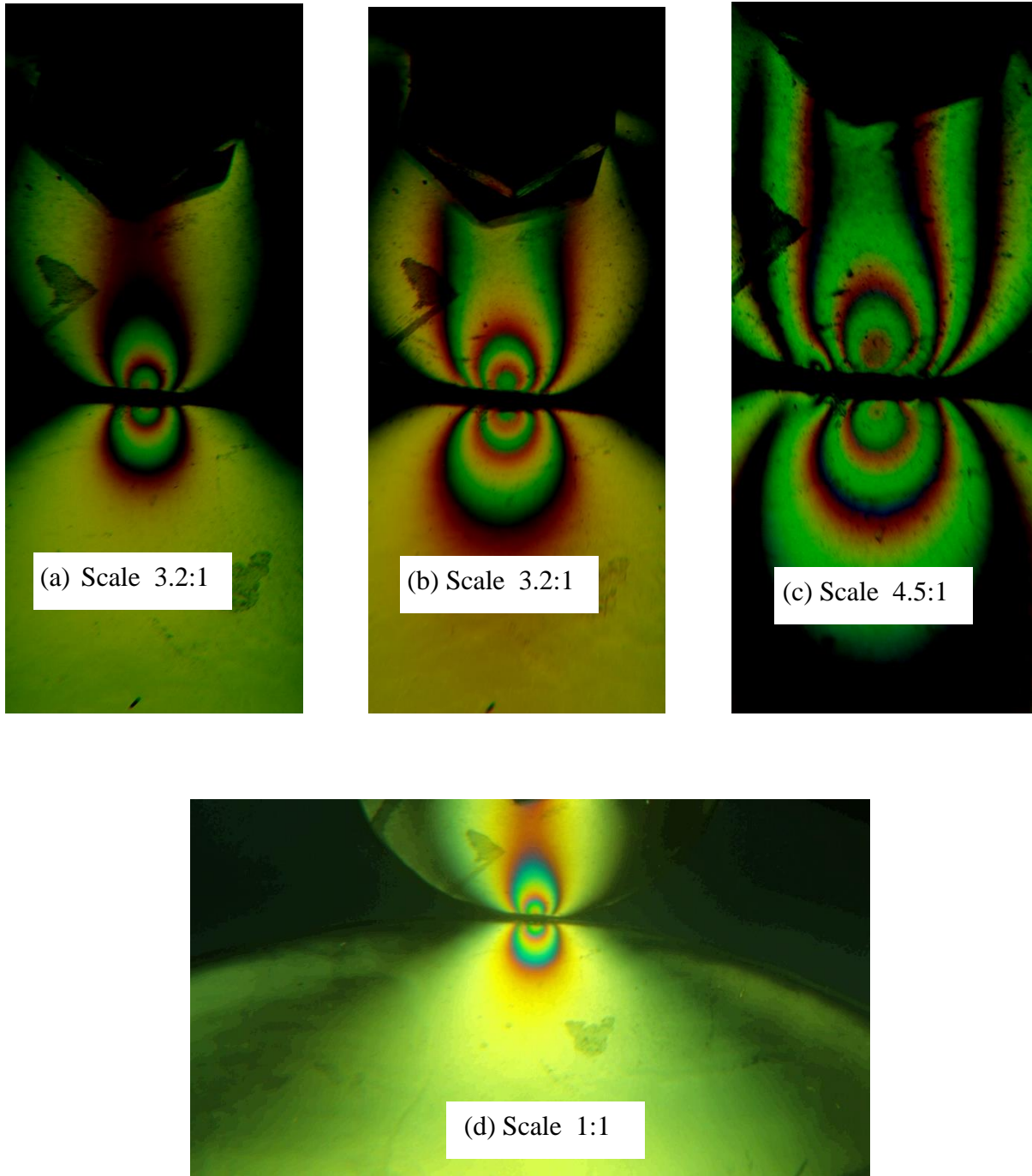**Figure 14.** Y- component cam deformation

213

Figure 15. Photo elastic stress pattern when the load is
(a) 0.2 Kg , (b) 0.3 Kg , (c) 0.4 Kg, (d) 0.2 Kg with scale 1:1